Applied Catalysis B: Environmental 226 (2018) 565–574

Contents lists available at ScienceDirect

Applied Catalysis B: Environmental

journal homepage: www.elsevier.com/locate/apcatb

New insights into the mechanism of NH_3-SCR over Cu- and Fe-zeolite catalyst: Apparent negative activation energy at high temperature and catalyst unit design consequences

Saurabh Y. Joshi*, Ashok Kumar, Jinyong Luo, Krishna Kamasamudram, Neal W. Currier, Aleksey Yezerets*

Corporate Research and Technology, Cummins Inc., 1900 McKinley Avenue, Columbus, IN 47201, USA, USA

ARTICLE INFO

Keywords:
Diesel emission control
Kinetic model
Selective catalytic reduction of NOx
Ammonia SCR
$DeNO_x$

ABSTRACT

We demonstrate an unusual behavior of a practically-important reaction of selective catalytic reduction (SCR) of NO_x with NH_3 over a state-of-the-art Cu-SSZ-13 catalyst. In response to increasing temperature, the rate of SCR reaction increases initially, attains a maximum around 300 °C, and then declines, resulting in a negative apparent activation energy at higher temperatures. This behavior has never been previously reported because the side reaction of NH_3 oxidation obfuscated the kinetic analysis of SCR reaction at high temperatures. We were able to discover this phenomenon by performing severe hydrothermal aging of the catalyst that suppressed the NH_3 oxidation activity without a significant change in the SCR activity. Further, we show that the phenomenon is more general and also found in other Cu- and Fe-exchanged zeolite and V_2O_5-$(WO_3)/TiO_2$ catalysts. The behavior is explained based on the fact that the activation energy for NH_3 desorption is higher than that for standard SCR reaction. Therefore, at higher temperatures, the increase in the SCR reaction rate constant with temperature gets outpaced by the decline in the NH_3 coverage, resulting in the overall decline of the reaction rate.

One of the implications of the finding is that the studied Cu-SSZ-13 SCR catalyst never operates in a purely external mass transfer limited regime, under the range of conditions relevant to the practical SCR applications. In other words, there is always a certain contribution of slower reaction rate to the performance of the SCR catalyst, even after increasing the reaction rates by increasing catalyst amount, using the "fast" SCR reaction, or operating at elevated temperatures. This has significant consequences for the design of practical SCR catalysts, in particular related to the choices of the active material loading and channel hydraulic diameter, as empirically and analytically demonstrated in this paper.

1. Introduction

Selective catalytic reduction (SCR) technology has been used worldwide for the control of NO_x emissions in exhaust gases from stationary sources and automobiles. The SCR reaction consists of reduction of NO_x by NH_3 to form water and nitrogen. SCR catalysts were first installed in 1970s on industrial and utility plants in the form of V_2O_5-$(WO_3)/TiO_2$ based catalytic monoliths [1]. More recently, zeolite based Fe- or Cu-SCR catalysts have been used for automotive applications due to their high NO_x conversion efficiency and thermal durability [2]. A number of literature studies reported the mechanism of SCR reaction and it was shown that the SCR process can proceed via the following three pathways, depending on the ratio of NO and NO_2 in the feed NOx [1–11].

- Standard SCR reaction: This reaction takes place when NO is the only NOx species.

$$4NH_3 + 4NO + O_2 \rightarrow 4N_2 + 6H_2O$$

- Fast SCR reaction: Many studies have shown that the maximum SCR activity can be achieved with an equimolar mixture of NO and NO_2 [4,11].

$$2NH_3 + NO + NO_2 \rightarrow 2N_2 + 3H_2O$$

- NO_2-SCR reaction: This reaction is important when the feed NOx comprises mostly NO_2, and is often referred to as "slow" SCR pathway.

$$4NH_3 + 3NO_2 \rightarrow 3.5N_2 + 6H_2O$$

* Corresponding authors.
E-mail addresses: Saurabh.Joshi@cummins.com (S.Y. Joshi), aleksey.yezerets@cummins.com (A. Yezerets).

https://doi.org/10.1016/j.apcatb.2017.12.076
Received 13 August 2017; Received in revised form 20 December 2017; Accepted 31 December 2017
Available online 03 January 2018
0926-3373/

Nomenclature

A_i	preexponential factor for reaction i $\left(\frac{\text{mol}}{m^3_{washcoat}\,s}\right)$
$C_{fm,j}$	Cup-mixing concentration of species j in gas phase (mol/m^3)
$C_{s,j}$	Concentration of species j in washcoat (mol/m^3)
Cp_w	Specific heat capacity of solid (J/kg/K)
D_f	Diffusivity of species in bulk gas phase (m^2/s)
D_{wc}	Diffusivity of species in washcoat (m^2/s)
D_{Hf}	Hydraulic diameter of open flow area (m)
E_i	Activation energy for reaction i (J/mol)
j	Species (NH_3,NO,NO_2)
k_i	rate constant for reaction i $\left(\frac{\text{mol}}{m^3_{washcoat}\,s}\right)$
k_{me}	Bulk mass transfer coefficient
Nu	Dimensionless heat transfer coefficient
R_i	Rate of reaction i $\left(\frac{\text{mol}}{m^3_{washcoat}\,s}\right)$
$\bar{u}$	Average gas velocity in the channel (m/s)
T_f	Gas phase temperature (K)
T_s	Temperature of washcoat/substrate (K)
t	Time (s)
y_j	Mole fraction of species j in gas phase
$y_{s,j}$	Mole fraction of species j at gas-washcoat interface
x	Coordinate in radial direction in the washcoat
z	Axial coordinate

Greek letters

α_f (α_w)	Thermal diffusivity of gas (solid)
ε_{wc}	Void fraction of washcoat
δ_{wc}	Washcoat thickness $= \frac{A_{wc}}{P_\Omega} = \frac{cross-sectional\ area\ of\ washcoat}{wetted\ perimeter}\,(m)$
ν_{ij}	Stoichiometric coefficient of species j in reaction i
Ω	Site density for NH_3 adsorption $\left(\frac{moles\ of\ NH_3}{m^3 washcoat}\right)$
θ_{NH3}	Fractional coverage of NH_3
ρ_w	Density of solid (kg/m^3)

Along with these primary reactions, additional side reactions can occur. NH_3 oxidation is a key side reaction consuming NH_3 at higher temperature.

$$4NH_3 + 3O_2 \rightarrow 2N_2 + 6H_2O$$

Further, presence of elevated NO_2 fraction in the feed NOx at low temperatures may lead to the formation of ammonium nitrate.

The afore-mentioned confounding reaction-network complicates the kinetic analysis of the SCR process. Therefore many researchers have followed the approach of determining kinetic parameters of individual reaction in isolation, as described below. Tronconi et al. [12] presented a global kinetic model for NO_x reduction over V_2O_5-(WO_3)/TiO_2 catalyst. The authors first determined the kinetics of NH_3 adsorption-desorption and independently estimated the kinetics of standard SCR reaction. Some other researchers [13–15] presented similar approach of global kinetic modeling for vanadia-based SCR catalysts. This modeling approach was extended to metal-exchanged zeolite catalyst by many researchers [4,6,10,11,16]. For Cu-ZSM-5 catalyst, Baik et al. [16] presented a global kinetic model for standard SCR reaction under steady state conditions, whereas, Olsson et al. [11] presented a comprehensive model considering transient effects and NO-to-NO_2 ratio. There are some other kinetic modeling studies predicting the transient behaviors of NH_3-SCR process on Fe-zeolite catalysts [17–19]. Further, Metkar et al. [6] developed comprehensive global kinetic models for NH_3-SCR over Fe-ZSM-5 and Cu-chabazite (CHA) catalysts including external and internal mass transfer effects. Recently, there are some fundamental studies on kinetics and mechanism over commercially popular Cu-SSZ-13 and Fe-SSZ-13 catalyst [3,20]. Bates et al. [3] measured standard SCR rate over Cu-SSZ-13 for various Cu/Al ratios using differential conversion conditions (< 20% conversion) and temperatures below 200 °C. Combined with density functional theory, the authors showed that standard SCR reaction primarily occurs on isolated Cu species located in six-membered ring of the SSZ-13 structure. Gao et al. [20] studied SCR reaction kinetics on Fe-SSZ-13 catalyst and showed that the catalyst is thermally durable and possesses high-temperature SCR activity.

Remarkably, in these published studies, the kinetics of SCR reaction was determined by focusing on the low temperature region (< 300 °C). Nevertheless, some reports analyzed the external and internal mass transfer effects in certain SCR catalysts. For example, Ruggeri et al. [21] showed the importance of internal and external mass transfer limitations in V_2O_5-(WO_3)/TiO_2 extruded catalyst, by comparing its SCR activity to the same catalyst in the powder form. Metkar et al. [22] showed existence of internal mass transfer limitations for standard SCR reaction over model Fe-ZSM-5 (> 350 °C) and Cu-ZSM-5 (> 250 °C) catalysts. Furthermore, they showed that internal mass transfer limitations were more prominent for the fast SCR reaction over broader temperature range (200–550 °C).

However, kinetics of SCR reaction at higher temperatures remained under-analyzed due to confounding factors, especially related to the side reaction of NH_3 oxidation by O_2. While low-temperature operation is critically important to the practical application, it is no less essential to understand the controlling process for SCR performance during high-temperature operation. In particular, in certain applications such as on-highway diesel engines, the design of SCR catalyst unit is focused around the most challenging high-flow conditions, encountered at high temperatures. In this work, we show that practically important SCR reaction exhibits an unusual behavior at higher temperature. Specifically, we demonstrate that the rate of SCR reaction over a state-of-the-art Cu-SSZ-13 catalyst increases initially, attains a maximum around 300 °C, and subsequently declines as the temperature is increased. In other words, the SCR reaction exhibited an apparent negative activation energy in the upper end of the practical temperature range. As a result, the studied Cu-SSZ-13 catalyst never operates in pure external mass transfer limited regime, under the range of operating conditions relevant to practical SCR applications. Initially, we discovered this phenomenon by pretreating the catalyst at high-temperature (800 °C – 4 h), which significantly decreased NH_3 oxidation activity, thus removing a major complicating factor for our kinetic analysis. Eventually, we demonstrated the validity of the same finding for other metal-exchanged zeolite and V_2O_5-(WO_3)/TiO_2 catalysts.

The objective of this work was to apply a combination of experimental studies and kinetic modeling to provide insights into the aforementioned phenomenon. The main challenge in the kinetic analysis of SCR process at high temperature was the occurrence of the side reaction of NH_3 oxidation by O_2. Our modeling approach was to determine the intrinsic kinetics of individual reactions by de-convoluting the overall NO_x reduction process. We utilized 1 + 1 dimensional monolithic reactor model considering external and internal mass transfer. Energy balance and gas phase concentrations were solved in the axial direction only, whereas mass balance in the washcoat was solved in axial and transverse (perpendicular to flow) direction.

2. Experimental

2.1. Catalyst samples and pre-treatment

Cylindrical samples (approximately 1 inch diameter by 1.5 inch

Table 1
Properties of Catalyst samples Used in the Present Work.

Sample	LxD (inch)	Cells/inch^2	Washcoat loading (g/inch^3)	Average waschcoat thickness (μm)
S1	1.5 × 1	600	2	55
S2	1.5 × 1	600	3.4	109
S3	1.5 × 1	300	2	80

length) were cored from a state-of-the-art Cu-SSZ-13 SCR catalyst purchased from the market. The measured Si/Al and Cu/Al ratios were ~9.5 and 0.3 respectively. This translates to the Cu loading of 484 μmol/g (or 3.1 wt%) of washcoat material. The average crystallite size was 2 μm as measured by SEM. The other properties of the catalyst samples are listed in Table 1. Unless mentioned otherwise, pretreatment for the samples was carried out by flowing synthetic exhaust gas containing 10% O_2, 8% H_2O, 7% CO_2 and the balance of N_2 at the gas hourly space velocity of 80,000 h^{-1} at 800 °C for 4 h. Compared to the practical application, such pretreatment corresponds to very harsh aging conditions, employed in this work to emphasize the explored kinetic behaviors. Additionally, we studied the effect of key design variables, such as cell density and catalyst loading on SCR performance; these experiments also provided insights into the SCR mechanism.

2.2. Reactor set-up

The bench flow reactor experimental set-up used in this work is the same as that described in detail in our earlier work [8]. In short, the catalyst sample was wrapped in Interam® mat which was compressed between the core and the quartz reactor tube. This prevented any gas from bypassing the catalyst periphery during the experiments. The temperatures of the catalyst and gas were measured by Omega K-type thermocouples. The catalyst inlet and outlet temperatures were measured by thermocouples located 3 mm inside the catalyst from the inlet and outlet faces, respectively. All gases were metered by MKS mass flow controllers calibrated for their respective gas species and flow range requirements. The effluent from the flow reactor was analyzed using an FT-IR spectrometer (MKS 2030 Series).

2.3. Experimental methodology

The preliminary objective of the experimental testing was to provide insight into the unusual phenomenon where rate of SCR reaction decelerates above 300 °C. Therefore we conducted experiments to determine intrinsic kinetics of the relevant individual SCR functions, such as NH_3 adsorption and desorption, SCR reaction and NH_3 oxidation. Two different test protocols were utilized in this study: transient temperature programmed desorption (TPD) experiments were carried out to study the dynamics of NH_3 adsorption-desorption, while the four-step protocol developed by Kamasamudram et al. [9] was used to characterize the SCR functions. Basic components of diesel exhaust gas (10% O_2, 8% CO_2, 7% H_2O and balance of N_2) were present during the entire experiment, while NO_x and NH_3 were switched on and off. More details about the experimental methodology can be found in our earlier work [9]. Unless indicated otherwise, the experiments were conducted using sample S1, maintaining the gas hourly space velocity of 160,000 h^{-1} and using 200 ppm inlet concentration of NO_x and NH_3. The protocol was applied for the case of standard and fast SCR (NO_2/NOx = 0, 0.5 respectively) at various temperatures.

3. Mathematical model

3.1. Reactor model

The two primary goals of the data analysis and reactor modeling were to determine the intrinsic kinetics of key SCR functions, such as NH_3 storage, NH_3 oxidation and NO_x reduction, and to develop a comprehensive mathematical model, capable of describing the behavior of apparent negative activation energy of SCR reaction at higher temperatures.

The following assumptions were made while developing the model: (i) uniform radial flow distribution so a single representative channel could be modeled; (ii) laminar flow, consistent with low Reynolds number characteristic of such applications (typically < 200); (iii) uniform catalyst coating across the monolith. The equations used in the model were based on our recent work [10]. The model consists of the species balance (Eqs. (1)–(3)) and energy balance (Eqs. (4) and (5)).

$$\frac{\partial C_{fm,j}}{\partial t} = -\bar{u}\frac{\partial C_{fm,j}}{\partial z} - \frac{4k_{me,j}}{D_{\mathrm{Hf}}}(C_{fm,j} - C_{s,j}) \tag{1}$$

$$\varepsilon_{wc}\frac{\partial C_{s,j}}{\partial t} = D_{wc,j}\frac{\partial^2 C_{s,j}}{\partial x^2} + \sum_i \nu_{ij} R_i \tag{2}$$

$$\Omega_k \frac{\partial \theta_k}{\partial t} = \sum \nu_j R_v, \tag{3}$$

$$\frac{\partial T_f}{\partial t} = -\bar{u}\frac{\partial T_f}{\partial z} - \frac{4\alpha_f Nu}{D_{Hf}^2}(T_f - T_s) \tag{4}$$

$$\frac{\partial T_s}{\partial t} = \alpha_w \frac{\partial^2 T_s}{\partial z^2} + \frac{h}{\delta_w \rho_w Cp_w}(T_f - T_s) + \frac{\delta_{wc}\sum_i R_i(-\Delta H_i)}{\delta_w \rho_w Cp_w} \tag{5}$$

The subscript j represents the species (j = NH_3, NO, NO_2), $C_{fm,j}$ is cup-mixing concentration of species j in gas phase, $C_{s,j}$ concentration of species j at gas-washcoat interface. The other symbols and notations used in the above equations are elaborated in the nomenclature Section. The diffusivity in the washcoat was assumed to be 10 times lower than that in the gas phase [10]. The governing Eqs. (1)–(5) were solved using commercial software, AVL BOOST® (Version 2016). We could obtain a grid-independent solution using 20 elements along the channel and 5 elements across the washcoat layer. During the transient simulations for NH_3-TPD, a time-step of 1 s was used.

3.2. Kinetic model

In this work, we have followed a global kinetic modeling approach based on the previously published studies [4,6,10,11,16]. The reactions considered and rate expressions are listed in Table 2. Arrhenius equation was used to capture temperature dependence of all the rate constants: $k_i = A_i e^{-E_i}/RT$. The kinetic parameters of individual reactions such as NH_3 storage, NH_3 oxidation and NO_x reduction, were determined in isolation, as described in detail in the subsequent section. This allowed us to minimize the number of parameters to be determined at once. Furthermore, we did not need to use an optimization

Table 2
Network of reactions and the rate expressions.

Reaction	Rate expression	Eq. number
$NH_3 + S \leftrightarrow NH_3 - S$	$R_1 = k_{f1} y_{s,NH3}(1 - \theta_{NH3}) - k_{b1}\theta_{NH3}$	(6)
$4NH_3 - S + 3O_2 \rightarrow 2N_2 + 6H_2O + 4S$	$R_2 = k_2 \theta_{NH3}[y_{O2}]$	(7)
$4NH_3 - S + 4NO + O_2 \rightarrow 4N_2 + 6H_2O + 4S$	$R_3 = k_3 \theta_{NH3} y_{NO}$	(8)

Table 3
Values of Arrhenius kinetic parameters used in modeling.

Reaction	k_i	A_i	Value of A_i (mol/m^3 washcoat/s)	E_i	Value of E_i (kJ/mol)
NH_3 adsorption on site S (R_{f1})	k_{f1}	A_{f1}	7.09×10^4	E_{f1}	0
NH_3 desorption on site S(R_{b1})	k_{b1}	A_{b1}	4.17×10^{12}	E_{b1}	$128(1–0.31\,\theta_{NH3})$
NH_3 oxidation (R_2)	k_2	A_2	1.5×10^{13}	E_2	150
Standard SCR (R_3)	k_3	A_3	4.5×10^{12}	E_3	84

package for parameter estimation, instead the intrinsic parameters were determined from individual experiments. The numerical values of the Arrhenius parameters are listed in Table 3.

Several researchers have developed global kinetic model for NH_3 adsorption-desorption considering one adsorption site [4,6,10,11,16]. Busco et al. [23] and Felix et al. [24] performed calorimetric measurements of ammonia adsorption on HZSM-5 and showed that the heat of adsorption is a function of surface coverage of NH_3. Further, Wilken et al. [25,26] performed similar micro-calorimeter measurements on Cu-BEA catalyst and showed that the heat of adsorption varied between 75 and 120 kJ/mol depending upon the NH_3 coverage. This effect has been modeled by several researchers considering Temkin-type adsorption isotherm [$E_b = E_b^0(1 - \alpha\theta_{NH_3})$] [4,6,10,11,16,27]. Our rate expression for NH_3 adsorption-desorption is based on these literature studies and is shown by Eq. (6) in Table 2. The site density for NH_3 adsorption was determined from NH_3-TPD experiment as discussed in detail in Section 4.3.1.

A number of researchers have modeled SCR and NH_3 oxidation reactions considering one active site where strongly adsorbed NH_3 reacts with gas-phase or weakly adsorbed NO_x and O_2 [6,10,11,15,21]. Our rate expressions for NH_3 oxidation (Eq. (7)) and standard SCR reaction (Eq. (8)) are consistent with these studies. It should be noted that NH_3 was selectively oxidized to N_2 and water during our NH_3 oxidation experiment, which is in agreement with literature reports [6,11,12,21].

4. Results and discussion

4.1. Unconventional behavior of NH_3-SCR

Fig. 1 illustrates the effect of hydrothermal aging on NH_3-SCR performance of the studied catalyst under the standard SCR conditions (feed $NO_2/NOx = 0$), following two different pretreatments. First, the catalyst was subjected to mild aging (commonly referred to as "degreening") at 550 °C for 4 h, followed by NH_3-SCR experiment, the results of which are represented by the open (○) markers. Subsequently, the same catalyst was hydrothermally aged at 800 °C for 4 h, and retested under the identical conditions. The results for that severely aged catalyst are represented using the filled markers (●). The performance of the degreened catalyst can be described as being conventional. The NH_3 conversion increased monotonically with temperature, whereas NO_x conversion increased with temperature initially and then declined above 350 °C due to the well-known side reaction of NH_3 oxidation. This behavior agrees well with numerous literature studies [6,9–11,15].

However, hydrothermally aged catalyst showed unusual behavior above 300 °C, such that not only the NO_x conversion, but also the NH_3 conversion decreased with temperature. Furthermore, the difference between the degreened and aged performance was larger at higher temperatures, as shown in Fig. 1. According to the conventional wisdom, NH_3 conversion should have increased monotonically with temperature because the reactions that consume NH_3 (namely, SCR and oxidation) are irreversible, and the species diffusivity also increases with the temperature.

4.2. Key hypotheses

We formulated and evaluated the following hypotheses, in an attempt to reconcile the above experimental observations: (i) the reaction was controlled by equilibrium at high temperatures, or (ii) external or internal mass transfer limitations were important, or (iii) reaction rate actually declined at high temperatures, forcing the process back to the kinetic control.

The equilibrium constants and thermodynamic parameters for SCR and NH_3 oxidation reactions have been reported by Centeno et al. [28]. The authors showed that the reactions can be considered as irreversible because the equilibrium constants are infinitely large ($K_{eq} > e^{200}$). Thus the first hypothesis can be ruled out.

To investigate the validity of the second hypothesis, we conducted NH_3-SCR experiment on a dual-layer catalyst, in which a Pt layer was deposited underneath an otherwise identical Cu-Zeolite SCR catalyst. Such dual-layer catalysts are commonly used for selective catalytic oxidation of ammonia slip, referred as AMOx. Fig. 2 shows the comparison of NH_3 conversions during NH_3-SCR experiments carried out on the SCR and AMOx catalysts. As can be seen, NH_3 conversion was significantly higher over the AMOx catalyst, because the bottom Pt layer provided additional high activity for NH_3 oxidation. In fact, NH_3 conversion reached nearly 100% over the AMOx catalyst above 350 °C, indicating that the external as well as the internal mass transfer through the SCR layer were sufficiently fast to supply NH_3 to the bottom Pt layer. This experiment conclusively proved that neither external nor internal mass transfer were the controlling mechanism, responsible for

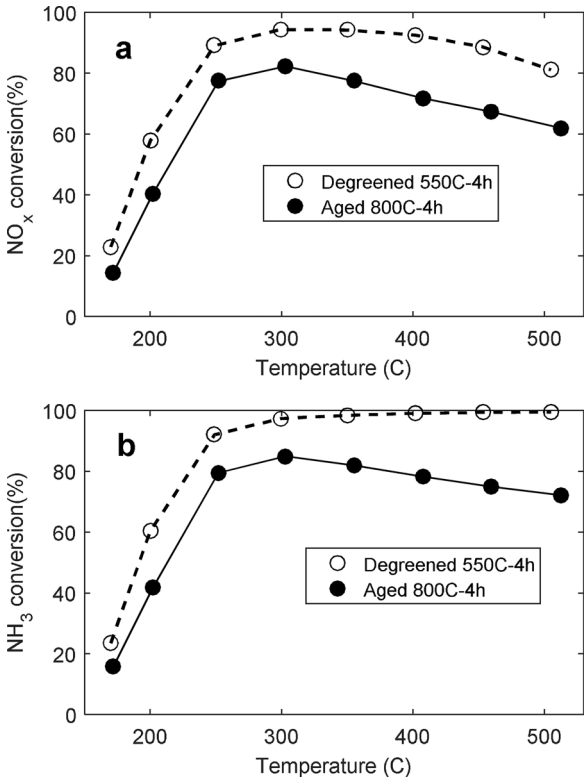

Fig. 1. Effect of hydrothermal aging on NH_3-SCR over Cu-SSZ-13 catalyst with $NO_2/NO_x = 0$. Feed: 200 ppm of NO and 200 ppm of NH_3 along with basic components of exhaust gas (10% O_2, 8% CO_2, 7% H_2O and balance of N_2), where (a) is steady state NOx conversion and (b) is steady state NH_3 conversion as a function of catalyst temperature.

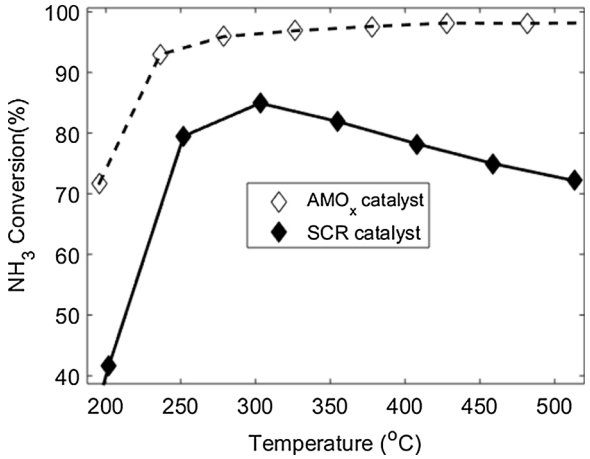

Fig. 2. Steady state NH_3 conversion during NH_3-SCR experiments over Cu-SSZ-13 SCR catalyst and AMOx catalyst aged at 800C for 4 h. Feed: 200 ppm of NO and 200 ppm of NH_3 along with basic components of exhaust gas (10% O_2, 8% CO_2, 7% H_2O and balance of N_2).

the unusual behaviors described above. This conclusion is further corroborated by the quantitative analysis of characteristic times of the controlling processes, as elaborated in Section 4.4.

4.3. Kinetic modeling showing the decrease in SCR reaction rate at higher temperatures

Having ruled out the first two hypotheses mentioned above, we concentrated on verifying the third hypothesis, by isolating the key SCR functions and determining their intrinsic kinetics as elaborated in the subsequent section.

4.3.1. Ammonia adsorption-desorption

We determined the kinetics of adsorption-desorption utilizing temperature-programmed desorption (TPD) protocol, as shown in Fig. 3. First, the catalyst was exposed to the gas flow containing 220 ppm NH_3 at 150 °C for sufficient duration (~1 h) to achieve saturation. Then, NH_3 feed was shut off for 10 min, maintaining the same temperature (150 °C) to remove any weakly stored NH_3. Finally, the temperature was ramped to 500 °C at the rate of 10 °C/min and all the remaining NH_3 was desorbed. The amounts of NH_3 stored and released were quantified, and mass balance within 5% was achieved.

As can be seen from Fig. 3, we were able to model the data very well using one-site model considering Temkin-type isotherm (Eq. (6)), as described in detail in the kinetic model section. The coverage dependent activation energy for desorption was determined to be $128(1–0.31\,\theta_{NH3})$ kJ/mol, where θ_{NH3} is coverage of NH_3 on the surface. Several authors reported similar value for heat of adsorption for zero coverage ranging from 120 to 130 kJ/mol [23,24,26]. The kinetic parameters of NH_3 adsorption-desorption thus derived (and described in Table 3 and Table 4) were kept constant throughout the subsequent steps of modeling.

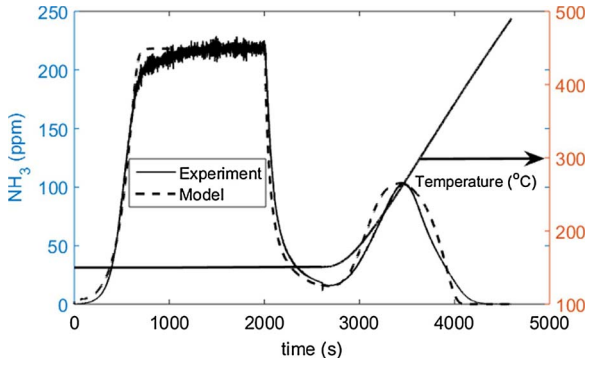

Fig. 3. NH_3 evolution with time during the temperature programmed desorption study. Feed NH_3 = 220 ppm along with other components of exhaust gas (8% CO_2, 7%H_2O and balance of N_2). The catalyst temperature is plotted on the secondary axis.

Table 4
Values of other parameters used in modeling.

Parameter	Value	Unit
Ω	890	mol/m^3 washcoat

4.3.2. NH_3 oxidation

NH_3 oxidation experiment was carried out with the feed consisting of 200 ppm of NH_3 along with basic components of exhaust gas. The markers in Fig. 4 show experimental results for steady-state NH_3 conversion in the reaction of its oxidation by oxygen. The activation energy for NH_3 oxidation was determined to be 150 kJ/mol, which is in agreement with the value reported in literature studies [10,11]. However, the absolute NH_3 conversion was lower than the reported values, consistent with much more severe aging used in our study. In fact, as will be shown in the Section 4.6.1, the severe aging used in our study suppressed the overall NH_3 oxidation activity of the catalyst, but preserved the activation energy of that process. This proved important to our efforts to de-couple this effect from other reactions occurring on the catalyst at high temperatures.

4.3.3. Standard SCR reaction

As a starting point, a simplified kinetic model for standard SCR reaction was developed, based on our experimental data and literature information, focused on differential conversion at temperatures below 200 °C. In particular, Fig. 5 shows the Arrhenius plot for our data for the studied SCR catalyst. The resulting activation energy of 84 kJ/mol is in agreement with the literature studies [6,10,11]. Several studies reported that rate of standard SCR reaction on Fe- and Cu-zeolite catalysts is first-order with respect to NO and zero-order to that of NH_3 [29–32]. Using these parameters in power law model (Eq. (9)); the experimental data was modeled over the entire temperature range; as shown in Fig. 6.

$$R_{SCR} = A_0 exp\left(\frac{-84{,}000}{8.314T}\right)NO \tag{9}$$

As can be seen, the model matched the data very well below 250 °C but significantly over-predicted the conversions at higher temperatures. Furthermore, the model predicted monotonically increasing conversion with temperature but the experimental data showed decreasing conversion above 300 °C. These observations indicated that some

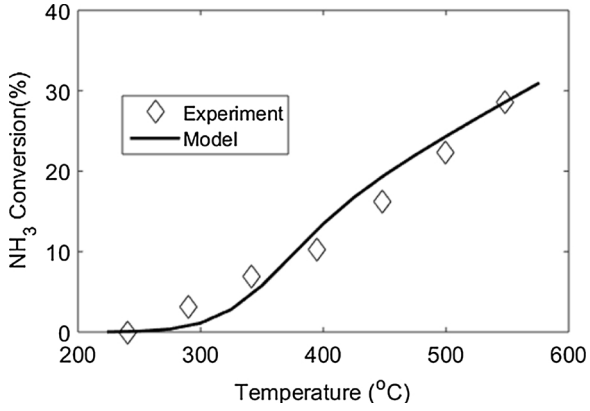

Fig. 4. Steady-state NH_3 conversion as a function of temperature during NH_3 oxidation reaction. Feed: 200 ppm of NH_3 along with basic components of exhaust gas (10% O_2, 8% CO_2, 7% H_2O and balance of N_2).

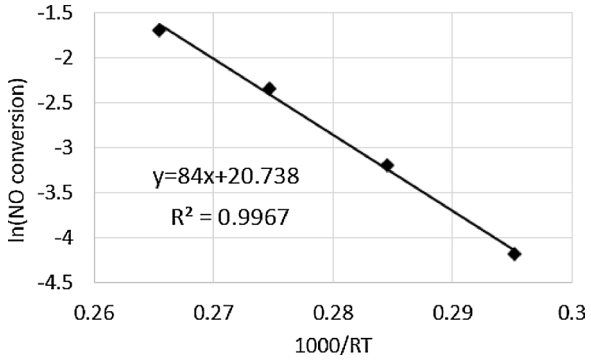

Fig. 5. Arrhenius plot for Cu-SSZ-13 SCR catalyst during standard SCR conditions. Feed: 200 ppm NO, 200 ppm NH_3 along with basic components of exhaust gas (10% O_2, 8% CO_2, 7% H_2O and balance of N_2). The temperature range used for the plot was 407–453 K.

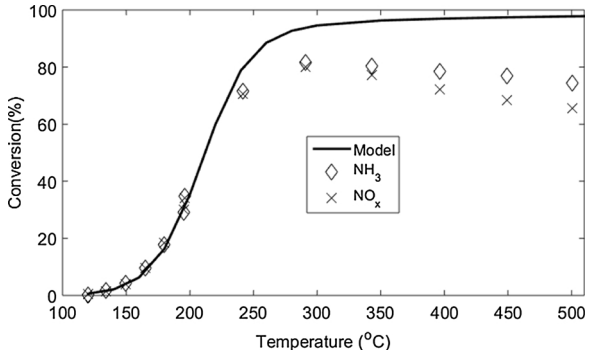

Fig. 6. Steady-state conversions as a function of temperature during standard SCR reaction. Feed: 200 ppm NO, 200 ppm NH_3 along with basic components of exhaust gas (10% O_2, 8% CO_2, 7% H_2O and balance of N_2). Markers represent experimental data and curve represents modeling result obtained using the power law model.

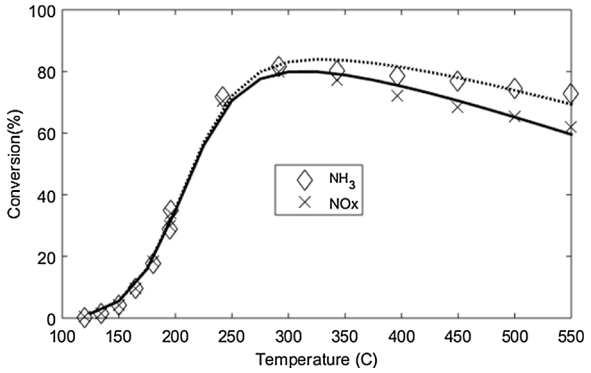

Fig. 7. Steady-state NO_x and NH_3 conversions as a function of temperature during standard SCR reaction. Feed: 200 ppm NO, 200 ppm NH_3 along with basic components of exhaust gas (10% O_2, 8% CO_2, 7% H_2O and balance of N_2). Markers represent experimental data and curves represent modeling results obtained using the detailed model.

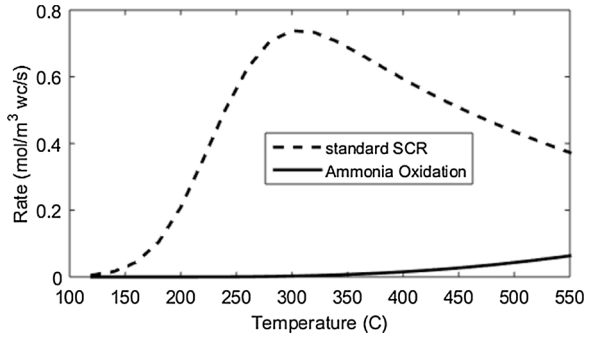

Fig. 8. Calculated rates of various reactions under standard SCR conditions. The reaction rates vary along the length of catalyst. The plot shows simulated reaction rates at 50% length (where local S.V. is 320,000/h).

additional mechanisms became important at higher temperatures. We have then incorporated in the model the additional mechanisms of NH_3 storage and NH_3 oxidation (Eqs. (6) and (7)), which are essentially inconsequential at low temperatures because of the pseudo 0th order and negligible activity, respectively [29–32]. As a result, good agreement between data and model was achieved, as evident from Fig. 7.

It is instructive to de-convolute the contribution of individual reactions by a superposition of their calculated rates, as shown in Fig. 8. For the purposes of this comparison, we have plotted the calculated reaction rates at 50% of the catalyst length, corresponding to the local space velocity of 320,000/h. As can be seen in Fig. 8, standard SCR reaction was dominant over the entire temperature range. Interestingly, the rate of standard SCR reaction increased initially, attained a maximum and dropped as temperature was increased. To elaborate this unusual phenomenon, we plotted rate constants and fractional NH_3 coverage (θ) in Fig. 9. The rate constants increased exponentially with temperature following the Arrhenius dependence. However, θ dropped sharply with temperature due to exponential increase in the rate of desorption. Specifically, at higher temperatures, the rate of desorption outpaced the rate of standard SCR due to its higher activation energy (128 kJ/mol) than standard SCR (84 kJ/mol). As a result, the rate of standard SCR reaction decreased at higher temperatures. This combination of factors was therefore responsible for the apparent negative activation energy above 300 °C.

4.4. Unusual regime transition: kinetic to mixed to kinetic regime

In order to gain further insights into the controlling process over a range of operating conditions, it is instructive to compare characteristic times for reaction, external and internal mass transfer. The characteristic time for reaction (t_R), external mass transfer ($t_{MT,e}$), internal mass transfer ($t_{MT,i}$), are defined as $\frac{D_{Hf} C_s}{4\delta_{wc} R_3}$, $\frac{D_{Hf}^2}{16 D_f}$, $\frac{\delta_{wc}^2}{D_{wc}}$ respectively. Here, D_{Hf} is hydraulic diameter of open flow area, C_s is concentration, δ_{wc} is washcoat thickness, R_3 is rate of standard SCR reaction, D_f is diffusivity of NO in fluid phase, D_{wc} is diffusivity of NO in the washcoat. Fig. 10 shows the characteristic times as a function of temperature for different processes. The characteristic times for external and internal mass transfer decreased monotonically with temperature since the diffusion coefficients slightly increased with temperature. Interestingly, the reaction time decreased initially, attained a minimum around 300 °C then increased, as temperature was increased. The curve for reaction time can be seen as a mirror-image of the reaction rate (Fig. 8) due to their inverse dependence. Fig. 10 is useful to determine the governing process as a function of temperature. The process with largest characteristic time represents overall bottleneck and governs the conversion. Following the criteria developed by Joshi et al. [33], the catalyst operates in a kinetic regime when characteristic reaction time is an order of magnitude higher than other times (specifically, $t_R > 10 t_{MT,e}$ and $t_R > 10 t_{MT,i}$). The reaction time was significantly higher than other characteristic times, below 200 °C. This indicated that the standard SCR reaction was much slower than the other processes and the catalyst operated in a kinetic regime below 200 °C. Further, the catalyst operated in a mixed regime in the intermediate temperature range (250–550 °C), where the rates of all the processes were comparable. Eventually, reaction time became significantly larger again above 550 °C and the catalyst transitioned back to the kinetic regime. To our knowledge, this phenomenon has not been reported in the literature, where the performance of Cu-zeolite SCR catalyst transitioned from kinetic to mixed to kinetic regime, as temperature was increased. This behavior was attributed to non-monotonic dependence of reaction rate on temperature.

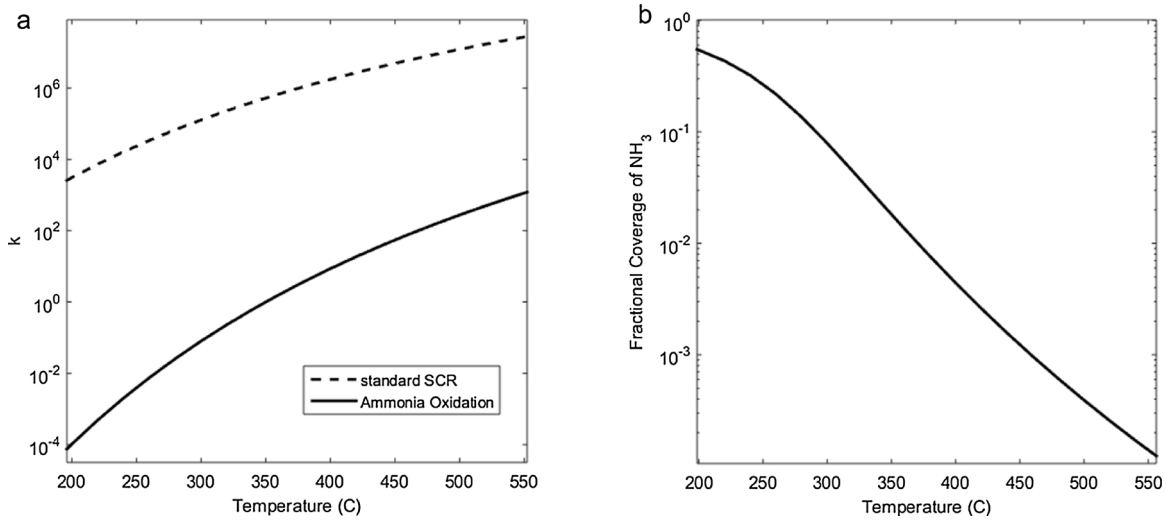

Fig. 9. (a) Calculated rate constants for standard SCR and ammonia oxidation reactions. (b) Calculated fraction coverage of NH_3 during standard SCR reaction at 50% length (where local S.V. is 320,000/h).

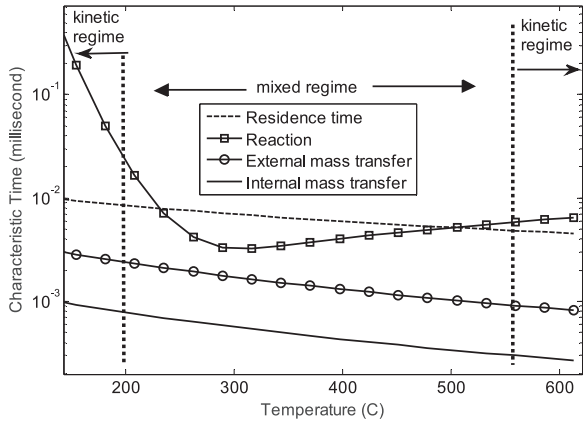

Fig. 10. Calculated characteristic times as a function of temperature under standard SCR conditions. Feed: 200 ppm NO, 200 ppm NH_3 along with basic components of exhaust gas (10% O_2, 8% CO_2, 7% H_2O and balance of N_2).

4.5. Verifiable consequences of the proposed hypothesis

The above results are conclusively pointing to the fact that the rate of standard SCR reaction decelerates at elevated temperatures because NH_3 desorption outpaces the increase in the reaction rate constant. This hypothesis should have a number of experimentally verifiable consequences, which we will examine below by varying such practically-relevant catalyst design parameters as catalyst loading on the monolith and channel hydraulic diameter.

4.5.1. Effect of catalyst loading

We conducted two sets of NH_3-SCR experiments using catalyst samples, S1 and S2. As shown in Table 1, all the parameters except catalyst loading were identical during the experiment. S1 is the same SCR catalyst as used through the aforementioned experimental study, S2 is chemically identical, however has 70% higher loading of the catalyst material on the monolith.

Fig. 11 shows the impact of catalyst loading on steady-state conversions under the standard SCR conditions (feed $NO_2/NO_x = 0$). For the case of a monolithic catalyst sample consisting of catalytically active material in the form of a washcoat, an increase in the loading of catalytic components enhances the conversion at lower temperatures where reaction is the rate limiting step [33,34]. As temperature is increased while carrying out an irreversible reaction on the monolithic

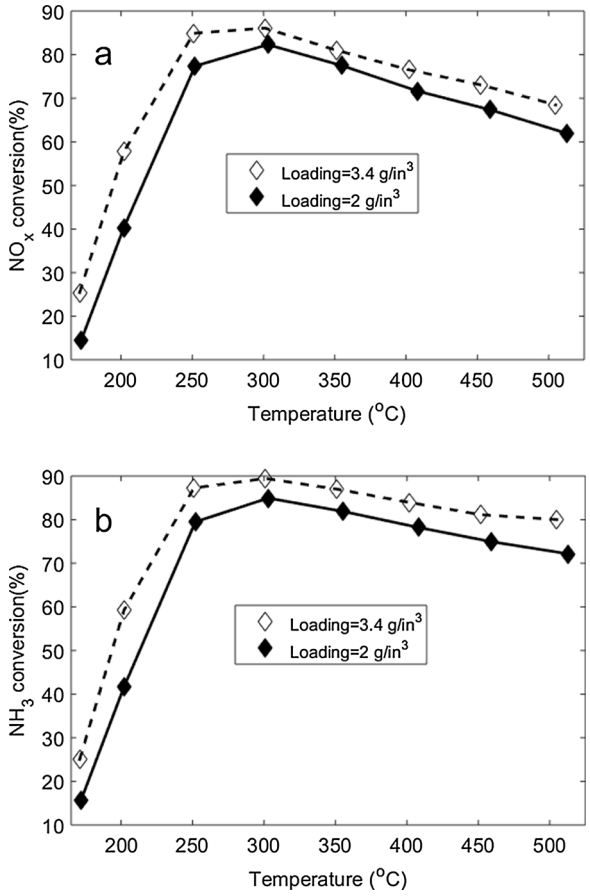

Fig. 11. Effect of catalyst loading on NH_3-SCR over Cu-SSZ-13 catalyst. Feed: 200 ppm of NO and 200 ppm of NH_3 along with basic components of exhaust gas (10% O_2, 8% CO_2, 7% H_2O and balance of N_2), where (a) is steady state NOx conversion and (b) is steady state NH_3 conversion as a function of catalyst temperature.

catalyst, the reaction rate increases following Arrhenius dependence and the impact of loading of catalytic component becomes less important. Eventually, at sufficiently high temperature, the reaction becomes infinitely fast and conversion is entirely controlled by external mass transfer where the catalytic component loading has practically no impact on conversion [33,34]. But the results shown in Fig. 11 are rather contrary to the conventional principles. The increase in the

loading of catalytic components enhanced the conversion initially, but the impact of the loading was minimal at the intermediate temperatures around 300 °C. Most surprisingly, the impact of the loading became more significant as temperature was further increased above 400 °C. These results further corroborate our finding that the studied catalyst undergoes a transition from kinetic to mixed and then back to the kinetic regime, in response to increasing temperature.

4.5.2. Effect of channel hydraulic diameter

A monolithic catalyst consists of a uniform matrix of a large number of parallel channels through which reacting fluid flows and catalytically active material is deposited in the form of a washcoat on the channel wall. These monolithic channels are usually referred as cells. The channel hydraulic diameter is determined by cell density, defined as number of cells per square inch (cpsi). To study the impact of channel hydraulic diameter, we conducted NH_3-SCR experiment using two samples S1 and S3. As shown in Table 1, the samples had identical catalytically active material and only differed by the cell density. Fig. 12 shows the impact of cell density on conversions during standard SCR.

For a monolithic catalyst, as cell density is increased, the channel diameter becomes smaller. As a result, external mass transfer is enhanced due to smaller external diffusion distance. Thus for a given catalyst loading, higher cell density should enhance the conversion in external mass transfer limited regime where the reaction rate is fast. On the other hand, when the performance is limited by slower reaction rate in kinetic regime, there is practically no effect of cell density on conversion [33,34]. As shown in Fig. 12, higher cell density has indeed enhanced the conversion at intermediate temperatures around 300 °C indicating that the rate of SCR reaction was highest around 300 °C and external mass transfer became important. In contrast, the impact of cell density was minimum at lower and higher temperatures indicating that the conversion was governed by the slower reaction rate. These results once again substantiate our earlier finding that the SCR reaction undergoes an unusual transition from kinetic to mixed to kinetic regime, as temperature is increased.

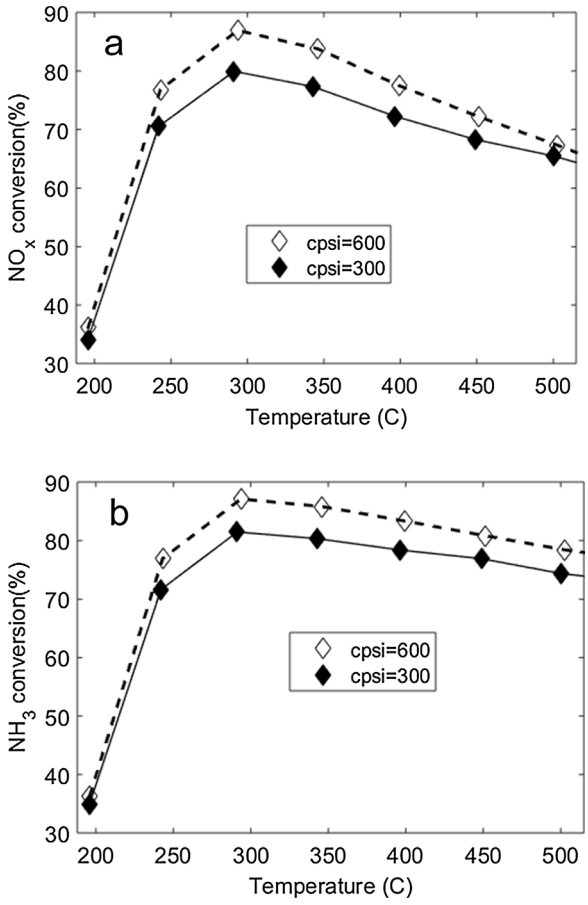

Fig. 12. Effect of cell density on NH_3-SCR over Cu-SSZ-13 catalyst under standard SCR conditions. Feed: 200 ppm NO and 200 ppm of NH_3 along with basic components of exhaust gas (10% O_2, 8% CO_2, 7% H_2O and balance of N_2), where (a) is steady state NOx conversion and (b) is steady state NH_3 conversion as a function of catalyst temperature.

4.6. Extension of the phenomenon to other SCR catalysts

As shown above, the studied Cu-SSZ-13 catalyst operates in a regime of kinetic control at high temperatures (> 550 °C). However, our analysis does not preclude dominance of external or internal mass transfer limitations during high-temperature operation of some SCR catalysts, as reported by some researchers [21,22]. For example, extruded SCR catalysts have longer internal diffusion length compared to washcoated monolith catalysts [21,34]. As a result, the dominance of internal mass transfer limitations were demonstrated for the case of V_2O_5-(WO_3)/TiO_2 extruded catalyst [21]. Metkar et al. [22] observed internal mass transfer limitations during SCR reaction at elevated temperatures on Fe- and Cu-ZSM-5 monolithic catalysts. Thus, in certain cases, SCR catalyst may not transition to kinetic regime at high temperature. Nevertheless, our finding of apparent negative activation energy of SCR reaction at high temperature, is more general, as demonstrated in this section.

Kinetics of NH_3-SCR reaction has been extensively studied in the literature for Cu-zeolite [3,6,10,11,20], Fe-zeolite [6,35] and V_2O_5-$(WO_3)/TiO_2$ [12–14] catalysts. Collectively, these studies reported apparent activation energy for standard SCR reaction in the range from 70 to 85 kJ/mol. Furthermore, some authors determined activation energy for NH_3 desorption for zero coverage in the range from 120 to 130 kJ/mol [23,24,26]. These values of activation energies are in close agreement with the values determined in this work for Cu-SSZ-13 catalyst. More importantly, this combination of activation energies should result in apparent negative activation energy for SCR reaction at higher temperatures. Thus our finding can be extended to other metal-exchanged zeolite and V_2O_5-$(WO_3)/TiO_2$ catalysts. This phenomenon is commonly overlooked in several literature studies due to obfuscating factor of NH_3 oxidation reaction [6,7,10–22]. In this section, we demonstrate the extension of the phenomenon to other catalyst types, aging states and fast SCR conditions.

4.6.1. Generalization of the phenomenon for the catalyst in its fresh state

Fig. 13 shows the impact of hydrothermal aging on NH_3 oxidation activity. As can be seen, the NH_3 oxidation activity was significantly suppressed for severely aged catalyst. However, mildly degreened sample showed significantly higher NH_3 oxidation activity that obfuscated the kinetic analysis of SCR reaction at high temperatures. Therefore we de-convoluted NH_3 oxidation reaction to perform kinetic analysis of SCR process, as described below. Figure SI-1a shows conversions during standard SCR reaction over Cu-SSZ-13 catalyst sample mildly pretreated at 550 °C for 4 h. The markers represent experimental data whereas curves show modeling results; the kinetic parameters are listed in Table 5. As can be seen, the NO_x and NH_3 conversions were identical below 350°C. But there was significant over-consumption of NH_3 at higher temperatures due to NH_3 oxidation reaction. The calculated rates of standard SCR and NH_3 oxidation reactions are shown in Figure SI-1a'. Standard SCR reaction is dominant below 350 °C whereas NH_3 oxidation reaction becomes important at higher temperatures. Interestingly, the rate of standard SCR reaction drops sharply at higher temperatures. In the previous literature studies, this drop has been attributed to the side reaction of NH_3 oxidation [6,7,9–11,21,22]. However, we showed that there exist an additional mechanism, responsible for the drop in rate of SCR reaction at higher temperatures, related to the de-population of surface NH_3. For this purpose, we modeled the data again by neglecting NH_3 oxidation reaction; the results are shown

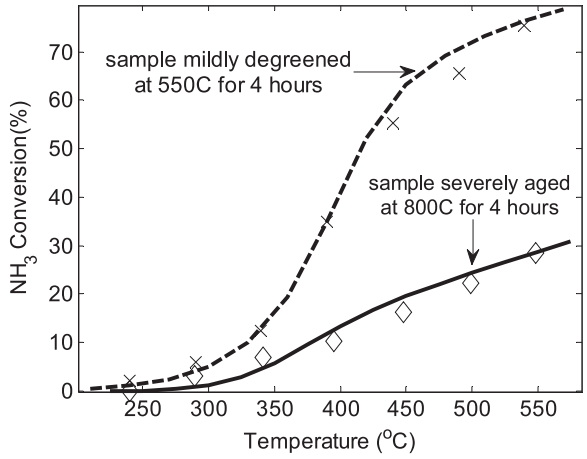

Fig. 13. Impact of hydrothermal aging on the NH_3 oxidation activity. Feed: 200 ppm of NH_3 along with basic components of exhaust gas (10% O_2, 8% CO_2, 7% H_2O and balance of N_2). Markers represent experimental data, whereas curves represent modeling result.

in Figure SI-1b. As can be seen, the modeled NO_x and NH_3 conversions were identical over the entire temperature range. The model predictions were excellent below 350 °C but they deviate from experimental data at higher temperatures since NH_3 oxidation reaction was not considered. Furthermore, this modeling analysis revealed that the rate of standard SCR reaction goes through a maximum around 300 °C as shown in Figure SI-1b'. We attribute the drop in SCR reaction rate above 350 °C to sharp desorption of NH_3 at higher temperatures. As expected, this result is very similar to that for severely aged catalyst sample as discussed in Section 4.3.3 and shown in Fig. 8.

Thus, the same phenomenon responsible for the apparent negative activation energy of SCR reaction, is likely taking place in a fresh catalyst as well, but it is commonly missed due to obfuscating factors related to the side reaction of NH_3 oxidation [6,7,9–11,21,22].

4.6.2. Fast SCR conditions

Here we show that fast SCR reaction over the Cu-SSZ-13 catalyst exhibited an apparent negative activation energy at higher temperatures. For this purpose, we carried out fast SCR reaction on two samples S1 and S3. These samples had identical catalytically active material and only differed by the cell density (or channel hydraulic diameter), as shown in Table 1. As shown in Figure SI-2, the NO_x and NH_3 conversions during fast SCR increased initially, attained maximum around 300 °C and eventually decreased as temperature was increased. Furthermore, higher cell density enhanced conversions below 350 °C. Remarkably, the impact of cell density kept on diminishing at higher temperatures. As discussed earlier in Section 4.5.2., higher cell density should enhance conversion in the external mass transfer limited regime, where reaction is extremely fast, however the cell density has practically no impact on conversion in kinetic regime [33,34]. Therefore it can be inferred from Figure SI-2 that the rate of fast SCR reaction increased initially, attained a maximum around 300 °C and eventually decreased, in response to the increasing temperature. In other words, fast SCR reaction also showed the apparent negative activation energy at higher temperatures. Furthermore, the impact of cell density was minimal around 550 °C as shown in Figure SI-2, indicating that the rate of fast SCR reaction dropped so low that it operated in the kinetic regime around 550 °C. We attribute this unusual behavior to NH_3 desorption outpacing the rate of fast SCR reaction at high temperature.

4.6.3. The most challenging case – fast SCR on a fresh catalyst

In an attempt to find conditions that would present the most challenge for the notion derived above that the SCR reaction is never fully free of the kinetic limitations; we have chosen the case which should yield the highest absolute rates and therefore the least chance of kinetic control: a degreened catalyst operating under fast SCR conditions.

Figure SI-3 shows conversions during fast SCR reaction over the Cu-SSZ-13 SCR catalyst degreened at 550 °C for 4 h. Interestingly, even in this case, the conversions were significantly lower than the external mass transfer limit over entire temperature range. In other words, there was always a certain contribution of the reaction kinetics, even at high temperature, with the optimal feed NO_2/NO_X ratio, and on a non-aged catalyst. These results are consistent with the above findings that the Cu-SSZ-13 catalyst does not operate in purely external mass transfer limited regime under many practical conditions.

4.6.4. Fe-zeolite

Finally, we show that the aforementioned behavior of Cu-zeolite SCR catalyst can also be found in Fe-zeolite SCR catalysts, depending on the catalyst aging state. Shwan et al. [36] studied the effect of hydrothermal aging on the kinetics of NH_3-SCR reaction over Fe-BEA SCR catalyst. The authors reported that the hydrothermal treatment (700 °C for 24 h) resulted in a significant loss of NH_3 oxidation functionality with a minor drop in the activity for SCR reactions. Further, they reported that NH_3 conversion under standard SCR conditions decreased with temperature above 400 °C. These reported observations are similar to our findings on the Cu-SSZ-13 catalyst.

Additionally, Metkar et al. [6] determined the kinetics of NH_3-SCR over Fe-ZSM-5 catalyst and reported activation energy of 70.5 kJ/mol for standard SCR reaction. They also reported coverage dependent activation energy of 145.9(1-0.97θ) kJ/mol for NH_3 desorption. This combination of activation energies would result in deceleration of the rate of SCR reaction at higher temperatures. We modeled the experimental data obtained from Metkar et al. [6]. Figure SI-4 (a) and (b) show modeled NO_x conversion and rate of standard SCR reaction using the kinetics reported by Metkar et al. [6]. The rate of standard SCR reaction decelerates as temperature is increased above 400 °C resulting in an apparent negative activation energy; similar to our findings for Cu-SSZ-13 catalyst.

5. Conclusions

We have provided novel insights into the mechanism of NH_3-SCR reaction over a state-of-the-art Cu-SSZ-13 catalyst. In particular, we have shown that the SCR reaction has an apparent negative activation energy at high temperatures. Despite numerous literature studies [3–22], this phenomenon remained undiscovered because the side reaction of NH_3 oxidation,

Table 5
Values of Arrhenius kinetic parameters for mildly pretreated Cu-SSZ-13 catalyst.

Reaction	k_i	A_i	Value of A_i (mol/m^3 washcoat/s)	E_i	Value of E_i (kJ/mol)
NH_3 adsorption on site S (R_{f1})	k_{f1}	A_{f1}	4.97×10^4	E_{f1}	0
NH_3 desorption on site S (R_{b1})	k_{b1}	A_{b1}	4.74×10^8	E_{b1}	$110(1–0.38\,\theta_{NH3})$
NH_3 oxidation (R_2)	k_2	A_2	2.4×10^{13}	E_2	150
Standard SCR (R_3)	k_3	A_3	1.8×10^{13}	E_3	84

particularly pronounced at high temperatures, complicated the kinetic analysis of the SCR reaction. We were able to discover this unusual behavior by carefully selecting pretreatment condition that selectively suppressed the NH_3 oxidation function without a significant change to the other SCR functions. As a result, SCR reaction was dominant over the entire operating temperature of 150–550 °C. The drop in SCR reaction rate at high temperature was then explained based on the NH_3 desorption outpacing the rate of SCR reaction with temperature. It should be noted that the kinetic parameters for various SCR processes were determined individually, rather than through a global fit. Moreover, these kinetic parameters are in close agreement with the values reported in several literature studies [6,10–14,20,23–26]. While discovered under particular set of conditions and for Cu-SSZ-13 catalyst, these findings were then generalized to the SCR reaction on other metal-exchanged zeolite and V_2O_5-(WO_3)/TiO_2 catalysts.

We have further showed that the resulting deceleration of SCR reaction rate at elevated temperatures translated into the transition back to the kinetic control regime, contrary to the conventional wisdom. These findings have substantial practical significance for SCR catalyst unit design for automobile applications. While low-temperature operation is important for catalyst ***formulation*** selection to achieve the activity light-off at sufficiently low temperatures, the ***catalytic unit design*** is primarily driven by the high-temperature conditions. This is because the highest flows in the engine are realized at the highest temperatures, consistent with the upper end of the range studied in this work. As we have illustrated, the practical consequences of our findings include an unconventional approach to choosing such unit design parameters as catalyst loading and cell density (channel diameter). In particular, while catalyst loading was expected to have no impact at elevated temperatures because of the expected external mass-transfer limited regime; we have shown that it can have substantial impact because of the kinetic or mixed control. Furthermore, cell density was expected to have a substantial impact at high temperatures where SCR reaction was expected to be so fast that the entire process should have been external mass-transfer limited; but the studied SCR catalyst never achieved true external mass transfer limited regime; even in fast SCR reaction on a mildly aged catalyst at the temperature as high as 500 °C. These findings are opening opportunities for further optimization of SCR catalyst units.

We have shown that the phenomenon of apparent negative activation energy of SCR reaction at high temperature, is more general and also found in other metal-exchanged zeolite and V_2O_5-(WO_3)/TiO_2 catalysts. However, our observation of SCR catalyst transitioning back to kinetically controlled regime at high temperature, may not be universal, especially for monolithic catalyst consisting of thicker washcoat or larger particle size, there can be a significant role of external and internal mass transfer limitations, as reported by some studies [21,22].

Acknowledgement

Authors would like to thank Mr. Randall Jines for his help with collecting the reactor data.

Appendix A. Supplementary data

Supplementary data associated with this article can be found, in the online version, at https://doi.org/10.1016/j.apcatb.2017.12.076.

References

[1] P. Forzatti, Appl. Catal. A: Gen. 222 (2001) 221–236.
[2] J.M. Fedeyko, H. Chen, T.H. Ballinger, E.C. Weigert, H. Chang, J.P. Cox, P.J. Andersen, SAE Paper, (2009) 2009-01-0899.
[3] Shane A. Bates, Anuj A. Verma, Christopher Paolucci, Atish A. Parekh, Trunojoyo Anggara, Aleksey Yezerets, William F. Schneider, Jeffrey T. Miller, W. Nicholas Delgass, H. Fabio, Ribeiro J.Catal. 312 (2014) 87–97.
[4] Massimo Colombo, Isabella Nova, Enrico Tronconi, Catal. Today 197 (15 December (1)) (2012) 243–255.
[5] Isabella Nova, Enrico Tronconi IFAC Proc. 42 (29) (2009) 183–190.
[6] P. Metkar, M. Harold, V. Balakotaiah, Chem. Eng. Sci. 87 (2013) 51–66.
[7] Hanna Sjövall, Richard J. Blint, Louise Olsson, Appl. Catal. B: Environ. 92 (19 October (1–2)) (2009) 138–153.
[8] C. Henry, K. Kamasamudram, N. Currier, A. Yezerets, M. Castagnola, H. Chen, SAE Paper, (2012) (2012-01-1084).
[9] K. Kamasamudram, N.W. Currier, A. Yezerets, Catal. Today 151 (2010) 212–222.
[10] S.Y. Joshi, A. Kumar, J. Luo, K. Kamasamudram, A. Yezerets, Appl. Catal. B: Environ. 165 (2015) 27–35.
[11] L. Olsson, H. Sjovall, R.J. Blint, Appl. Catal. B: Environ. 81 (2008) 203–217.
[12] E. Tronconi, L. Lietti, P. Forzatti, S. Malloggi, Chem. Eng. Sci. 51 (1996) 2965–2970.
[13] J.A. Dumesic, N.-Y. Topsoe, H. Topsoe, Y. Chen, T. Slabiak, J. Catal. 163 (1996) 409.
[14] R. Willi, B. Roduit, R.A. Koeppel, A. Wokaun, A. Baiker, Chem. Eng. Sci. 51 (11) (1996) 2897.
[15] D. Chatterjee, T. Burkhardt, M. Weibel, E. Tronconi, I. Nova, C. Ciardelli, SAE Paper, (2006) 2006-01-0468.
[16] J.H. Baik, S.D. Yim, I.-S. Nam, Y.S. Mok, J.H. Lee, B.K. Cho, S.H. Oh, Ind. Eng. Chem. Res. 45 (2006) 5258.
[17] S. Malmberg, M. Votsmeier, J. Gieshoff, N. Soger, L. Mußmann, A. Schuler, A. Drochner, Top. Catal. 42–43 (2007) 33.
[18] M. Colombo, I. Nova, E. Tronconi, L. Zimmermann, Appl. Catal. B: Environ. 111–112 (2012) 106–118.
[19] H. Sjovall, R.J. Blint, A. Gopinath, L. Olsson, Ind. Eng. Chem. Res. 49 (2010) 39–52.
[20] F. Gao, M. Kollár, R.K. Kukkadapu, N.M. Washton, Y. Wang, J. Szanyi, C.H.F. Peden, Appl. Catal. B: Environ. 164 (2015) 407–419.
[21] M.P. Ruggeri, I. Nova, E. Tronconi, Chem. Eng. J. 207–208 (2012) 57–65.
[22] P.S. Metkar, V. Balakotaiah, M.P. Harold, Chem. Eng. Sci. 66 (2011) 5192–5203.
[23] C. Busco, A. Barbaglia, M. Broyer, V. Bolis, G.M. Foddanu, P. Ugliengo, Thermochim. Acta 418 (2004) 3–9.
[24] S.P. Felix, C. Savill-Jowitt, D.R. Brown, Thermochim. Acta 433 (2005) 59.
[25] N. Wilken, et al., Appl. Catal. B: Environ. 111–112 (2012) 58–66.
[26] N. Wilken, et al., Catal. Today 151 (2010) 237–243.
[27] T.J. Wang, S.W. Baek, H.J. Kwon, Y.J. Kim, I.S. Nam, M.S. Cha, G.K. Yeo, Ind. Eng. Chem. Res. 50 (2011) 2850–2864.
[28] I. Mejía-Centeno, S. Castillo, R. Camposeco, G.A. Fuentes, Catal. Commun. 31 (2013) 11–15.
[29] H.Y. Huang, R.Q. Long, R.T. Yang, Appl. Catal. A: Gen. 235 (2002) 241–251.
[30] T. Komatsu, M. Nunokawa, I.S. Moon, T. Takahara, S. Namba, T. Yashima, J. Catal. 148 (1994) 427–437.
[31] P.S. Metkar, N. Salazar, R. Muncrief, V. Balakotaiah, M.P. Harold, Appl. Catal. B: Environ. 104 (2011) 110–126.
[32] R. Delahay, S. Kieger, N. Tanchoux, P. Trens, B. Coq, Appl. Catal. B Environ. 52 (2004) 251–257.
[33] S.Y. Joshi, M.P. Harold, V. Balakotaiah, Chem. Eng. Sci. 65 (2010) 1729–1747.
[34] R.M. Heck, R.J. Farrauto, S.T. Gulati, Catalytic Air Pollution Control: Commercial Technology, 3rd edition, Wiley, 2016.
[35] M. Iwasaki, K. Yamazaki, H. Shinjoh, Appl. Catal. A: Gen. 366 (2009) 84–92.
[36] S. Shwan, J. Jansson, J. Korsgren, L. Olsson, M. Skoglundh, Catal. Today 197 (2012) 24–37.